IEEE Access
Multidisciplinary | Rapid Review | Open Access Journal

Received September 28, 2020, accepted October 8, 2020, date of publication October 19, 2020, date of current version October 29, 2020.

*Digital Object Identifier 10.1109/ACCESS.2020.3031906*

# A Synchronization Approach Based on Bidirectional Correlation Search for Aperiodic Chaotic Direct Sequence Spread Spectrum Signals

**GUOGANG YUAN, ZILI CHEN, XIJUN GAO, JIANGYAN HE, AND HONGXIA JIA**
Department of UAV Engineering, Shijiazhuang Campus of AEU, Shijiazhuang 050003, China
Corresponding author: Zili Chen (chenzl_mec@163.com)

**ABSTRACT** The chaotic direct sequence spread spectrum (CD3S) is one of the distinguished techniques providing physical layer secrecy and low probability of intercept (LPI) in wireless communication. Due to the noise-like and aperiodic characteristics of chaotic signals, the synchronization of CD3S signals is a challenging issue. A synchronization approach for aperiodic CD3S signals based on bidirectional correlation search (BDCS) is proposed. Through a joint acquisition of forward frequency domain matched filtering (FDMF) and backward FDMF, the synchronization module aligns received CD3S signals with local chaotic sequences without aid of the pilot signal. The probability distribution of correlator output is derived with additive white Gaussian noise and narrowband jamming. The probability of detection, probability of false alarm, and bit error rate are analyzed mathematically. An approximate solution of the local optimal acquisition threshold coefficient is obtained. These theoretical analyses are verified by numerical simulations, the results of which demonstrate that the proposed synchronization approach enables the CD3S system to resist interception and adapt to the environment with low signal-to-noise and signal-to-jammer ratios.

**INDEX TERMS** Chaotic direct sequence spread spectrum (CD3S), synchronization, bidirectional correlation search, anti-interception, narrowband jamming, local optimal acquisition threshold coefficient.

## I. INTRODUCTION

Chaotic signals have attracted much attention in the field of secure communication due to their several distinct characteristics such as sensitivity to initial conditions, aperiodicity, and random-like behavior [1]–[4]. Chaotic direct sequence spread spectrum (CD3S) is an important application of chaotic signals in the field of secure communication, which was originally proposed by Heidari-Bateni [5] and Parlitz [6] simultaneously in 1994. CD3S is a spread spectrum technique using chaotic sequences instead of classical pseudo-noise (PN) sequences. Compared with direct sequence spread spectrum (DSSS) communication using PN sequences, CD3S communication has a lower probability of intercept [7] and a higher physical-layer security [8]. However, CD3S communication has not taken over the traditional DSSS communication after nearly two and half decades of research work on this topic [9]. Due to the aperiodicity of chaotic signals, it is difficult to realize the synchronization of CD3S signals through correlation operation. The synchronization problem restricts the development of CD3S communication.

In recent years, the research on the synchronization of CD3S signals mainly focuses on three directions: pilot aided synchronization (PAS), synchronization based on fixed chaotic sequence, and semi-blind demodulation based on state estimation. In the PAS approach, the PN sequences [10], [11] or truncated chaotic [12]–[15] sequence are utilized as additive pilot signal, where the synchronization is realized by searching the correlation peak of the pilot signal. In the researches of PAS, white Gaussian noise, jamming, and multiuser are widely concerned, and different methods are proposed to adapt to the complex channel. Compared with CD3S signals, the periodicity of pilot is an obvious feature that makes the transmitted signal easy to

The associate editor coordinating the review of this manuscript and approving it for publication was Xiaofan He.

be intercepted. In other words, the pilot benefits the synchronization but degrades the anti-interception performance of CD3S signals. In the second synchronization approach, the system applies a fixed chaotic sequence to spread all the transmitted bits [16], [17], and the synchronization can be realized by the synchronization technology of the DSSS system. The fixed CD3S systems are vulnerable to eavesdropping and interception. Reference [17] proposed a method called ''fake user'' to enhance the security of fixed CD3S system. The enhancement of anti-interception performance is not considered in [17]. The weak anti-interception performance of the pilot and fixed chaotic sequences makes the transmission parameters easy to be obtained by noncooperative receivers. Accordingly, targeted intelligent jamming can be implemented on the pilot and fixed chaotic sequences [18]. In the semi-blind demodulation approach, the receiver uses state observer such as Extended Kalman Filter (EKF) [19]–[22], Unscented Kalman Filter (UKF) [23]–[26], Chebyshev Polynomial Kalman Filter (CPKF) [27] or Particle Filter (PF) [28]–[30] to estimate chaotic sequence from the received signal. In the semi-blind demodulation approach, the receiver can demodulate the message bits without locally generating the same chaotic sequence as the transmitter. EKF and CPKF are suitable for estimating chaotic signals with piecewise linear phase trajectories in Gaussian noise. UKF is suitable for estimating chaotic signals with nonlinear phase trajectories in Gaussian noise. PF is suitable for estimating chaotic signals in non-Gaussian noise. In the semi-blind demodulation approach, the transmitted signals have a low probability of intercept because each message bit is spread by a unique chaotic sequence. However, the semi-blind demodulation requires prior knowledge of noise distribution and noise power, which is not easy to obtain in many scenarios. Moreover, the semi-blind demodulation cannot effectively utilize the correlation property of chaotic sequences, and jamming is usually not considered in semi-blind demodulation. Different models and estimators are applied to estimate chaotic codes and message bits from received signals, but the improvement in bit error rate (BER) performance is limited for semi-blind demodulation.

In order to construct a CD3S system with low intercept probability and anti-jamming capacity, this paper proposes a synchronization approach based on bidirectional correlation search (BDCS). In order to ensure the low intercept probability of the transmitted signal and facilitate the receiver to generate local chaotic codes, the transmitter uses two chaotic maps to generate chaotic spreading codes. The first chaotic map allocates chaotic initial values for each message bit, while the second generates chaotic spreading sequence according to the initial values of each bit. The key to ensure the anti-jamming capacity of the spread spectrum system is to separate the spread spectrum signals and jamming using the autocorrelation characteristics of the spreading sequence. For the DSSS system, the PN sequences are periodic. It is not necessary to consider the direction of correlation search when implementing synchronization. For the CD3S system, since the chaotic code is aperiodic, the synchronization can only be achieved when the correlation search direction points to the synchronization position. Considering that the received signal may lead or lag behind the local chaotic sequence, the receiver synchronizes the local chaotic spread spectrum sequence and the received signal by BDCS in this paper. The BDCS is performed through forward frequency domain matched filtering (FDMF) and backward FDMF.

The rest of this paper is organized as follows: Section II introduces the CD3S system model. In Section III, the synchronization approach based on BDCS is proposed. In Section IV, the mathematical model for the probability of detection and probability of false alarm is established, and the local optimal acquisition threshold coefficient is derived. Section V presents the numerical simulation results. Finally, some conclusions and suggestions for future work are given in Section VI.

## II. CD3S SYSTEM MODEL DESCRIPTION

Fig. 1 illustrates the CD3S system block schematic. The transmitter generates the CD3S signal. The CD3S signal is transmitted to the receiver through the delayed channel with additive Gaussian noise and jamming. The receiver synchronizes the local chaotic sequence with the received signal and demodulates the received signal. In Fig. 1, $b_k$ represents the $k$th message bit of the transmitter, $c_{0,1}$ represents the chaotic initial value of the system, $c_{k,m}$ represents the $m$th chip of the $k$th message bit, $v_n$ represents the white Gaussian noise, $j_n$ represents the jamming, $r_n$ represents the received signal, and $c'_{k,m}$ represents the local chaotic code.

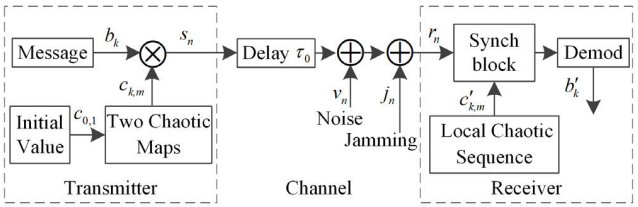


**FIGURE 1.** CD3S system block schematic.

Inspired by [31], the chaotic spreading code $c_{k,m}$ is generated by two chaotic maps. According to the system initial value $c_{0,1}$, the first chaotic map $f_1(c)$ generates the chaotic initial value $c_{k,1}$ corresponding to $b_k$. This process can be expressed as

$$c_{k,1} = f_1\left(c_{k-1,1}\right). \tag{1}$$

The second chaotic map $f_2(c)$ generates the chaotic spreading sequence $\left\{c_{k,m} | m = 1, 2, \cdots, \beta\right\}$ according to $c_{k,1}$, where $\beta$ is the spreading factor. This process can be expressed as

$$c_{k,m+1} = f_2\left(c_{k,m}\right). \tag{2}$$

The following three constraints need to be satisfied when generating chaotic spread spectrum sequences:

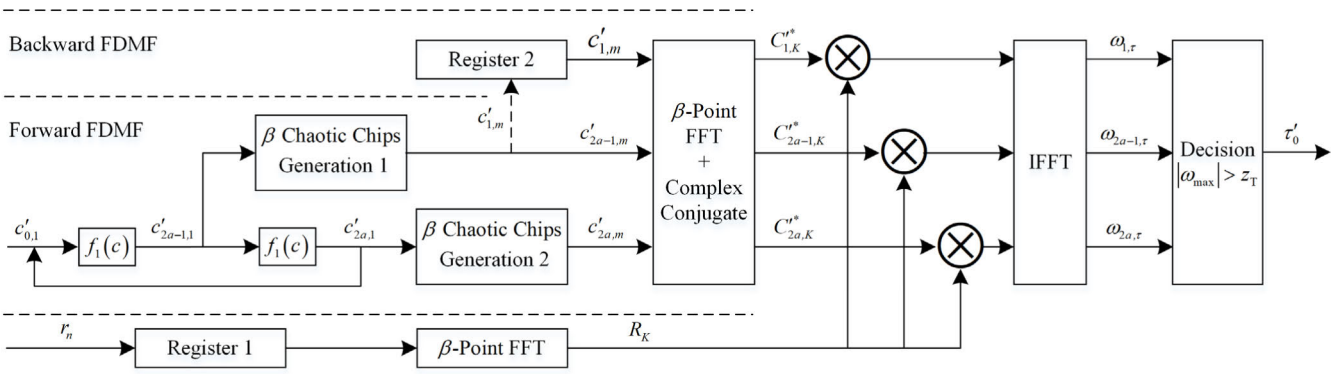


**FIGURE 2.** Flow chart of synchronization based on BDCS.

1) The system initial value $c_{0,1}$ should satisfy the initial value constraint of the first chaotic map $f_1(c)$;
2) $c_{k,1}$ generated by $f_1(c)$ should satisfy the initial value constraint of the second chaotic map $f_2(c)$;
3) $c_{k,m} \in [-1, 1]$.

When constraints (2) and (3) are not satisfied, linear transformation can be a method to solve the problem. In this paper, the first chaotic map uses Tent map which is given by

$$c_{k+1,1} = f_1(c_{k,1}) = \begin{cases} c_{k,1}/q, & 0 < c_{k,1} \le q \\ (1 - c_{k,1})/(1 - q), & q < c_{k,1} < 1 \end{cases} \quad (3)$$

where the Tent map parameter $q$ is in the range of $(0, 1)$, $c_{k,1} \in (0, 1)$.

The second chaotic map uses Logistic map which is given by

$$c_{k,m+1} = f_2(c_{k,m}) = 1 - 2(c_{k,m})^2, \quad (4)$$

where $c_{k,m} \in (-1, 1)$.

The transmitted CD3S signal $s_n$ is generated by multiplying $b_k$ and the chaotic spreading code $c_{k,m}$ as

$$s_n = s_{k,m} = b_k c_{k,m}, \quad (5)$$

where $n = (k-1)\beta + m$, $m = 1, 2, \cdots, \beta$.

## III. BIDIRECTIONAL CORRELATION SEARCH SYNCHRONIZATION APPROACH

In the CD3S system, synchronization includes two phases: acquisition and tracking. In the acquisition phase, the transmission delay is reduced to less than one chip period $T_c$. In the tracking phase, fine tuning is performed to remove the transmission delay within a chip duration.

Although the CD3S signals are aperiodic, the tracking of a CD3S signal is similar to that of the DSSS signal. Therefore, this paper only discusses the acquisition of CD3S signals and assumes that the transmission delay is a multiple of $T_c$. Based on the above analysis, the received signal $r_n$ can be expressed as

$$r_n = s_{n-\tau_0} + v_n + j_n, \quad (6)$$

where $\tau_0$ represents transmission delay.

For the DSSS system with periodic PN code, the acquisition can be completed by sliding correlation. For the CD3S system with aperiodic chaotic code, this approach can only complete the acquisition when the received signal lags behind the local spreading sequence. However, the received signal may lead or lag behind the local chaotic sequence, the acquisition approach of DSSS system is not applicable to CD3S system.

In this paper, BDCS is proposed to solve the acquisition problem. In the proposed approach, the forward FDMF can acquire the received signal when the received signal leads the local chaotic sequence, and the backward FDMF can acquire the received signal when the received signal lags behind the local chaotic sequence. Fig. 2 shows the flow chart of synchronization based on BDCS.

In Fig. 2, $c'_{k,m}$ represents the local chaotic spreading code, $c'_{0,1}$ represents the acquisition initial value, $a$ represents the rounds of correlation search, $\beta$ chaotic chips generation module 1 generates the local chaotic spreading sequence $\left\{c'_{2a-1,m} | m = 1, 2, \cdots, \beta\right\}$ according to the initial value $c'_{2a-1,1}$ and the second chaotic map $f_2(c)$, $\beta$ chaotic chips generation module 2 generates the local chaotic spreading sequence $\left\{c'_{2a,m} | m = 1, 2, \cdots, \beta\right\}$ according to the initial value $c'_{2a,1}$. Each time $\beta$ chips of $r_n$ are received, correlation search is performed once. Correlation search is achieved through FDMF. In the backward FDMF, the fixed chaotic spreading sequence $\left\{c'_{1,m} | m = 1, 2, \cdots, \beta\right\}$ is employed for backward correlation search. In the forward FDMF, the dynamically generated chaotic spreading sequences $\left\{c'_{2a-1,m} | m = 1, 2, \cdots, \beta\right\}$ and $\left\{c'_{2a,m} | m = 1, 2, \cdots, \beta\right\}$ are employed for forward correlation search. $\omega_{\max}$ is the maximum of $\left\{\omega_{1,\tau} | \tau = 1, 2, \cdots, \beta\right\}$, $\left\{\omega_{2a-1,\tau} | \tau = 1, 2, \cdots, \beta\right\}$, and $\left\{\omega_{2a,\tau} | \tau = 1, 2, \cdots, \beta\right\}$. $z_T$ is the acquisition threshold. The correlation search achieved by frequency-domain matched filtering can be expressed as

$$\omega_\tau = \sum_{n=0}^{\beta-1} r_n c'_{n-\tau} = \mathrm{IFFT}\left[R_K C'^*_K\right], \quad (7)$$

where $R_K = \mathrm{FFT}(r_n)$, $C'_K = \mathrm{FFT}(c'_n)$, $C'^{*}_K$ is the complex conjugate of $C'_K$.

The main steps of the synchronization process are described in Table 1.

**TABLE 1. Process of synchronization based on BDCS.**

**Step1.** Set the acquisition initial value $c'_{0,1}$=$c_{0,1}$.

**Step2.** Calculate $c'_{1,1}$ from $c'_{0,1}$ and $f_1(c)$. $\beta$ chaotic chips generation module 1 generates the fixed local chaotic spreading sequence $\{c'_{1,m} | 1 \le m \le \beta\}$ according to $c'_{1,1}$ .Store $\{c'_{1,m} | 1 \le m \le \beta\}$ in the register 2.

**Step3.** Receive $\beta$ chips of $r_n$ and perform correlation search once through FDMF. The backward FDMF is implemented by the fixed $\{c'_{1,m} | 1 \le m \le \beta\}$, and the forward FDMF is implemented by dynamically generated $\{c'_{2a-1,m} | 1 \le m \le \beta\}$ and $\{c'_{2a,m} | 1 \le m \le \beta\}$.

**Step4.** Determine whether $|\omega_{\max}|$ is greater than $z_{\mathrm{T}}$. If so, output delay estimation $\tau'_0$ to achieve acquisition. Otherwise, go to **step3**.

**Step5.** If the synchronization is interrupted when receiving $b_k$, set the acquisition initial value $c'_{0,1}$=$c_{k,1}$, and go to **step2.**

After synchronization, demodulation can be implemented by the following equation.

$$\hat{b}_k = \mathrm{sgn}\left(\sum_{m=1}^{\beta} r_{k,m} c_{k,m}\right). \tag{8}$$

## IV. THEORETICAL ANALYSIS OF PERFORMANCE

In this section, the probability distribution of correlator output with Gaussian white noise and narrowband jamming is modeled. Then, the false alarm probability and detection probability of BDCS-based synchronization are analyzed, and the approximate solution of local optimal acquisition threshold coefficient is derived. Finally, the BER of demodulation is analyzed.

### A. PROBABILITY DISTRIBUTION OF CORRELATOR OUTPUT

In the acquisition phase of synchronization, the output of each correlator can be expressed as

$$\begin{aligned}\omega_\tau &= \sum_{m=1}^{\beta} r_{N-\beta+m} c'_{k,m-\tau} \\ &= \sum_{m=1}^{\beta} s_{N-\beta+m} c'_{k,m-\tau} + \sum_{m=1}^{\beta} v_{N-\beta+m} c'_{k,m-\tau} \\ &\quad + \sum_{m=1}^{\beta} j_{N-\beta+m} c'_{k,m-\tau} \\ &= A + B + C,\end{aligned} \tag{9}$$

where $\{r_{N-\beta+m} | m = 1, 2, \cdots, \beta\}$ is the received signal. The variables in (9) are independent and identically distributed, and each variable has limited mean and variance. $\beta$ is a sufficiently large value ($\beta$ is usually greater than 500). According to the central limit theorem, $\omega_\tau$ approximately obeys the Gaussian distribution, which is denoted as $\omega_\tau \sim N(\mu_{\omega_\tau}, \sigma^2_{\omega_\tau})$. $\mu_{\omega_\tau}$ is the mean of $\omega_\tau$. $\sigma^2_{\omega_\tau}$ is the variance of $\omega_\tau$.

Since $A$, $B$, and $C$ are independent, $\mathrm{E}(B) = 0, \mathrm{E}(C) = 0$, the mean of $\omega_\tau$ can be expressed as

$$\mu_{\omega_\tau} = \mathrm{E}(A) + \mathrm{E}(B) + \mathrm{E}(C) = \mathrm{E}(A). \tag{10}$$

The variance of $\omega_\tau$ is given by

$$\begin{aligned}\sigma^2_{\omega_\tau} &= \mathrm{E}\left(\omega^2_\tau\right) - \mu^2_{\omega_\tau} \\ &= \mathrm{E}\left(A^2\right) + \mathrm{E}\left(B^2\right) + \mathrm{E}\left(C^2\right) - [\mathrm{E}(A)]^2.\end{aligned} \tag{11}$$

Since the variables in $B$ are independent and identically distributed, $\mathrm{E}(B) = 0$, $\mathrm{E}\left(B^2\right)$ can be expressed as

$$\begin{aligned}\mathrm{E}\left(B^2\right) &= \mathrm{E}\left[\left(\sum_{m=1}^{\beta} v_{N-\beta+m} c'_{k,m-\tau}\right)^2\right] \\ &= \mathrm{E}\left[\sum_{m=1}^{\beta} \left(v_{N-\beta+m} c'_{k,m-\tau}\right)^2\right] = \beta \frac{N_0}{2} P_{\mathrm{c}},\end{aligned} \tag{12}$$

where $N_0$ represents the single-sided power spectral density of white Gaussian noise $v_n$, and $P_{\mathrm{c}}$ represents the power of chaotic chip.

Assuming that the single-sided power spectral density of narrowband jamming $j_n$ is $N_{\mathrm{j}}$, the ratio of jamming bandwidth $B_{\mathrm{j}}$ to CD3S signal bandwidth $B_{\mathrm{s}}$ is $\gamma = B_{\mathrm{j}}/B_{\mathrm{s}}$, $\mathrm{E}\left(C^2\right)$ can be expressed as

$$\mathrm{E}\left(C^2\right) = \mathrm{E}\left[\sum_{m=1}^{\beta} \left(j_{N-\beta+m} c'_{k,m-\tau}\right)^2\right] = \beta\gamma \frac{N_{\mathrm{j}}}{2} P_{\mathrm{c}}. \tag{13}$$

When the probability density function of the second chaotic map $f_2(c)$ is known, $P_{\mathrm{c}}$ can be calculated as

$$P_{\mathrm{c}} = \int_{-\infty}^{+\infty} c^2 \rho(c) \mathrm{d}c, \tag{14}$$

where $\rho(c)$ is the probability density function of $f_2(c)$.

When $\rho(c)$ is unknown, $P_{\mathrm{c}}$ can be approximately calculated as

$$P_{\mathrm{c}} \approx \frac{1}{\beta} \sum_{m=1}^{\beta} c^2_{k,m}, \tag{15}$$

The values of $\mathrm{E}(A)$ and $\mathrm{E}\left(A^2\right)$ are related to the correlation between $s_n$ and $c'_{k,m}$.Due to the aperiodicity of CS3S signals, the proposed synchronization approach can only achieve partial alignment in the acquisition phase. Fig. 3 shows the schematic diagram of the partial alignment between $s_n$ and $c'_{k,m}$ in the acquisition phase, where the shadow part is the aligned area of $s_n$ and $c'_{k,m}$.

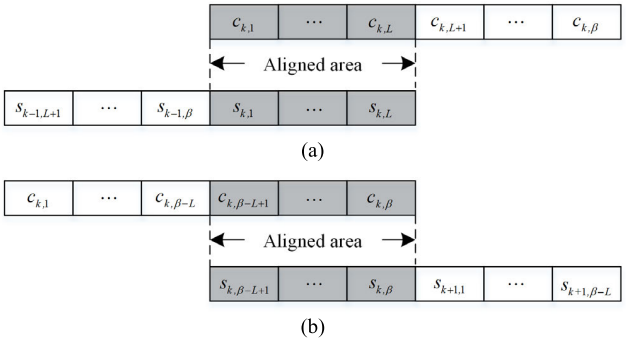


**FIGURE 3.** Schematic diagram of partial alignment between local chaotic sequence and CD3S signal. (a) Local chaotic sequence is aligned with the last $L$ chips of the received signal. (b) Local chaotic sequence is aligned with the first $L$ chips of the received signal.

In Fig. 3, the number of aligned chips is assumed to be $L$. For the situation shown in Fig. 3(a), $\mathrm{E}\left(A^2\right)$ can be calculated as

$$\begin{aligned}
&\mathrm{E}\left(A^2\right)\\
&= \mathrm{E}\left[\left(\sum_{m=1}^{L} s_{k,m}c_{k,m} + \sum_{m=L+1}^{\beta} s_{k-1,m}c_{k,m}\right)^2\right]\\
&= \mathrm{E}\left[\left(\sum_{m=1}^{L} s_{k,m}c_{k,m}\right)^2\right] + \mathrm{E}\left[\left(\sum_{m=L+1}^{\beta} s_{k-1,m}c_{k,m}\right)^2\right]\\
&\quad + 2\mathrm{E}\left[\left(\sum_{m=1}^{L} s_{k,m}c_{k,m}\right)\cdot\left(\sum_{m=L+1}^{\beta} s_{k-1,m}c_{k,m}\right)\right]\\
&= \mathrm{E}\left(\sum_{m=1}^{L} s_{k,m}^2 c_{k,m}^2 + \sum_{m=i+1}^{L}\sum_{i=1}^{L-1} s_{k,i}c_{k,i}s_{k,m}c_{k,m}\right)\\
&\quad + \mathrm{E}\left(\sum_{m=L+1}^{\beta} s_{k-1,m}^2 c_{k,m}^2\right)\\
&= L^2P_{\mathrm{c}}^2 + (\beta - L)P_{\mathrm{c}}^2. \qquad (16)
\end{aligned}$$

For the situation shown in Fig. 3(a), $\mathrm{E}(A)$ can be calculated as

$$\begin{aligned}
\mathrm{E}(A) &= \mathrm{E}\left(\sum_{m=1}^{L} s_{k,m}c_{k,m}\right) + \mathrm{E}\left(\sum_{m=L+1}^{\beta} s_{k-1,m}c_{k,m}\right)\\
&= b_k LP_{\mathrm{c}}. \qquad (17)
\end{aligned}$$

Equation (16) and (17) are also applicable to the situation in Fig. 3(b). Substituting (17) into (10), the mean value of $\omega_\tau$ is derived as

$$\mu_{\omega_\tau} = b_k LP_{\mathrm{c}}. \qquad (18)$$

Substituting (12), (13), (17) and (16) into (11), The variance of $\omega_\tau$ is derived as

$$\sigma_{\omega_\tau}^2 = (\beta - L)P_{\mathrm{c}}^2 + \beta\frac{N_0}{2}P_{\mathrm{c}} + \beta\gamma\frac{N_{\mathrm{j}}}{2}P_{\mathrm{c}}. \qquad (19)$$

### B. THE FALSE ALARM PROBABILITY OF SYNCHRONIZATION

A false alarm occurs when the local chaotic spreading sequence is not aligned with the received signal and the absolute value of correlation is greater than the acquisition threshold $z_{\mathrm{T}}$. Record the output of the correlator as $\omega_{\mathrm{u}}$ when the local chaotic spreading sequence and received signal are not aligned. In this case, $L = 0$. According to (18), it can be obtained that

$$\mu_{\omega_{\mathrm{u}}} = 0. \qquad (20)$$

According to (19), the following can be obtained

$$\sigma_{\omega_{\mathrm{u}}}^2 = \beta P_c^2 + \beta\frac{N_0}{2}P_{\mathrm{c}} + \beta\gamma\frac{N_{\mathrm{j}}}{2}P_{\mathrm{c}}. \qquad (21)$$

When the spectrum of message bits is spread, the bit energy $E_{\mathrm{b}}$ and noise power spectral density $N_0$ are constant. But the noise power in the system increases. To ensure that the signal-to-noise ratio (SNR) can reflect the relationship between signal power and noise environment, SNR is defined as the ratio of $E_{\mathrm{b}}$ to $N_0$, which is given by

$$S_{\mathrm{NR}} = \frac{E_{\mathrm{b}}}{N_0}. \qquad (22)$$

The bit energy $E_{\mathrm{b}}$ equals to

$$E_{\mathrm{b}} = \beta P_{\mathrm{c}}. \qquad (23)$$

In this paper, it is assumed that the jamming bandwidth is less than the bit bandwidth. When the message bits are spread, the jamming power in the system remains unchanged. Therefore, signal-to-jamming ratio (SJR) is defined as the ratio of signal power to jamming power, which is given by

$$S_{\mathrm{JR}} = \frac{E_{\mathrm{b}}/T_{\mathrm{b}}}{B_{\mathrm{j}}N_{\mathrm{j}}} = \frac{\beta P_{\mathrm{c}}}{B_{\mathrm{j}}N_{\mathrm{j}}}\cdot\frac{B_{\mathrm{s}}}{\beta} = \frac{P_{\mathrm{c}}}{\gamma N_{\mathrm{j}}}, \qquad (24)$$

where $T_{\mathrm{b}}$ is the bit period, $T_{\mathrm{b}} = \beta T_{\mathrm{c}} = \beta/B_{\mathrm{s}}$. Substituting (22) and (24) into (21), the following can be obtained

$$\sigma_{\omega_{\mathrm{u}}}^2 = E_{\mathrm{b}}^2\left(\frac{1}{\beta} + \frac{1}{2S_{\mathrm{NR}}} + \frac{1}{2\beta S_{\mathrm{JR}}}\right). \qquad (25)$$

The probability density function of $\omega_{\mathrm{u}}$ can be expressed as

$$f_{\mathrm{u}}(\omega_{\mathrm{u}}) = \frac{1}{\sqrt{2\pi}\delta_{\omega_{\mathrm{u}}}}\exp\left(-\frac{\omega_{\mathrm{u}}^2}{2\delta_{\omega_{\mathrm{u}}}^2}\right). \qquad (26)$$

The false alarm probability is derived as

$$\begin{aligned}
P_{\mathrm{F}} &= P\{|\omega_{\mathrm{u}}| \geq Z_{\mathrm{T}}\}\\
&= 2\int_{Z_{\mathrm{T}}}^{\infty} f_{\mathrm{u}}(\omega_{\mathrm{u}})\mathrm{d}\omega_{\mathrm{u}}\\
&= \mathrm{erfc}\left(\frac{Z_{\mathrm{T}}}{\sqrt{2}\delta_{\omega_{\mathrm{u}}}}\right), \qquad (27)
\end{aligned}$$

where $\mathrm{erfc}(x) = \frac{2}{\sqrt{\pi}} \int_x^{\infty} \exp\left(-u^2\right) \mathrm{d}u$ is the complementary error function. To simplify (27), the acquisition threshold coefficient is defined as

$$\alpha = \frac{Z_{\mathrm{T}}}{E_{\mathrm{b}}}. \tag{28}$$

Substituting (21) and (28) into (27), the following can be obtained

$$P_{\mathrm{F}} = \mathrm{erfc}\left[\alpha\left(\frac{2}{\beta} + \frac{1}{S_{\mathrm{NR}}} + \frac{1}{\beta S_{\mathrm{JR}}}\right)^{-\frac{1}{2}}\right]. \tag{29}$$

### C. THE DETECTION PROBABILITY OF SYNCHRONIZATION

Detection happens when $L$ ($L > 0$) chips of local chaotic spreading sequence are aligned with the received signal and the absolute value of correlation is greater than the acquisition threshold $z_{\mathrm{T}}$. Record the output of the correlator as $\omega_{\mathrm{s}}$ when the local chaotic spreading sequence and received signal are aligned. If $L$ bits are aligned in a certain correlation search, then $\beta - L$ bits will be aligned in an adjacent correlation search. Therefore, in the acquisition phase, the number of aligned chips will be in the range of $\left[\beta/2, \beta\right]$ in a certain correlation search, i.e., $L \in \left[\beta/2, \beta\right]$ when detection happens.

According to (18), it can be obtained that

$$\mu_{\omega_{\mathrm{s}}} = b_k L P_{\mathrm{c}} = b_k \frac{L E_{\mathrm{b}}}{\beta}. \tag{30}$$

According to (19), it can be obtained that

$$\begin{aligned}\sigma_{\omega_{\mathrm{s}}}^2 &= (\beta - L) P_{\mathrm{c}}^2 + \beta \frac{N_0}{2} P_{\mathrm{c}} + \beta \frac{N_{\mathrm{j}}}{2} P_{\mathrm{c}} \\ &= \frac{E_{\mathrm{b}}^2}{2}\left(\frac{2(\beta - L)}{\beta^2} + \frac{1}{S_{\mathrm{NR}}} + \frac{1}{\beta S_{\mathrm{JR}}}\right).\end{aligned} \tag{31}$$

The probability density function of $\omega_{\mathrm{s}}$ can be expressed as

$$f_{\mathrm{s}}(\omega_{\mathrm{s}}) = \frac{1}{\sqrt{2\pi}\delta_{\omega_{\mathrm{s}}}} \exp\left(-\frac{\left(\omega_{\mathrm{s}} - \mu_{\omega_{\mathrm{s}}}\right)^2}{2\delta_{\omega_{\mathrm{s}}}^2}\right). \tag{32}$$

No matter $b_k = 1$ or $b_k = -1$, the detection probability is the same when the noise and jamming conditions are the same. Assuming $b_k = 1$, in a single correlation search with $L$ chips aligned, the local detection probability $P_{\mathrm{d}}(L)$ is derived as

$$\begin{aligned}&P_{\mathrm{d}}(L) \\ &= P\{|\omega_{\mathrm{s}}| \geq Z_{\mathrm{T}}\} \\ &= \int_{Z_{\mathrm{T}}}^{\infty} f_{\mathrm{s}}(\omega_{\mathrm{s}}) \mathrm{d}\omega_{\mathrm{s}} + \int_{-\infty}^{-Z_{\mathrm{T}}} f_{\mathrm{s}}(\omega_{\mathrm{s}}) \mathrm{d}\omega_{\mathrm{s}} \\ &= \frac{1}{2}\mathrm{erfc}\left(\frac{Z_{\mathrm{T}} - \mu_{\omega_{\mathrm{s}}}}{\sqrt{2}\delta_{\omega_{\mathrm{s}}}}\right) + \frac{1}{2}\mathrm{erfc}\left(\frac{Z_{\mathrm{T}} + \mu_{\omega_{\mathrm{s}}}}{\sqrt{2}\delta_{\omega_{\mathrm{s}}}}\right) \\ &= \frac{1}{2}\mathrm{erfc}\left[\left(\alpha - \frac{L}{\beta}\right)\left(\frac{2(\beta - L)}{\beta^2} + \frac{1}{S_{\mathrm{NR}}} + \frac{1}{\beta S_{\mathrm{JR}}}\right)^{-\frac{1}{2}}\right] \\ &\quad + \frac{1}{2}\mathrm{erfc}\left[\left(\alpha + \frac{L}{\beta}\right)\left(\frac{2(\beta - L)}{\beta^2} + \frac{1}{S_{\mathrm{NR}}} + \frac{1}{\beta S_{\mathrm{JR}}}\right)^{-\frac{1}{2}}\right].\end{aligned} \tag{33}$$

In a large number of acquisition processes, it can be assumed that $L$ ($L \in \mathbf{N}$) obeys a uniform distribution in the range of $\left[\beta/2, \beta\right]$, Therefore, the global detection probability $P_{\mathrm{D}}$ can be expressed as

$$\begin{aligned}P_{\mathrm{D}} &= \sum_{L=\beta/2}^{\beta} \frac{1}{\beta - \frac{\beta}{2} + 1} P_{\mathrm{d}}(L) \\ &= \frac{2}{\beta + 2} \sum_{L=\beta/2}^{\beta} P_{\mathrm{d}}(L)\end{aligned} \tag{34}$$

### D. LOCAL OPTIMAL ACQUISITION THRESHOLD COEFFICIENT

According to equations (29) and (33), a higher acquisition threshold coefficient $\alpha$ means better false alarm probability performance and worse detection probability performance. It is important to set an appropriate acquisition threshold coefficient $\alpha$ to balance the false alarm probability performance and the detection probability performance. However, since (34) has no analytical solution, it is difficult to derive the global optimal solution for acquisition threshold coefficient. In the acquisition phase, missed detection will increase the synchronization time, while false alarm is relatively easy to identify by analyzing the subsequent output of the correlator. Therefore, the worst detection case (i.e., $L = \beta/2$) is considered and the local optimal solution of the acquisition threshold coefficient is derived in this case. In the following analysis, we assume $L = \beta/2$. According to (33), it can be obtained that

$$\begin{aligned}P_{\mathrm{d}}\left(\frac{\beta}{2}\right) &= \frac{1}{2}\mathrm{erfc}\left[\left(\alpha - \frac{1}{2}\right)\left(\frac{1}{\beta} + \frac{1}{S_{\mathrm{NR}}} + \frac{1}{\beta S_{\mathrm{JR}}}\right)^{-\frac{1}{2}}\right] \\ &\quad + \frac{1}{2}\mathrm{erfc}\left[\left(\alpha + \frac{1}{2}\right)\left(\frac{1}{\beta} + \frac{1}{S_{\mathrm{NR}}} + \frac{1}{\beta S_{\mathrm{JR}}}\right)^{-\frac{1}{2}}\right].\end{aligned} \tag{35}$$

As shown in (29) and (35), the false alarm probability and detection probability are related to the acquisition threshold coefficient $\alpha$, spreading factor $\beta$, $S_{\mathrm{NR}}$, and $S_{\mathrm{JR}}$. Set the false alarm probability index to $P_{\mathrm{FI}}$, according to (29), the minimum acquisition threshold coefficient $\alpha_{\min}$ that satisfies the index $P_{\mathrm{FI}}$ is derived as

$$\alpha_{\min} = \mathrm{erfc}^{-1}(P_{\mathrm{FI}})\left(\frac{2}{\beta} + \frac{1}{S_{\mathrm{NR}}} + \frac{1}{\beta S_{\mathrm{JR}}}\right)^{\frac{1}{2}}, \tag{36}$$

where $\mathrm{erfc}^{-1}(x)$ is the inverse complementary error function, $\mathrm{erfc}^{-1}[\mathrm{erfc}(x)] = x$.

It is assumed that the detection probability index when $L = \beta/2$ is set to $P_{\mathrm{dI}}$. In (35), the first term is much larger than the second term. Abandoning the second term of (35), the maximum acquisition threshold coefficient $\alpha_{\max}$ that satisfies the index $P_{\mathrm{dI}}$ is derived as

$$\alpha_{\max} \approx \frac{1}{2} + \mathrm{erfc}^{-1}(2P_{\mathrm{dI}})\left(\frac{1}{\beta} + \frac{1}{S_{\mathrm{NR}}} + \frac{1}{\beta S_{\mathrm{JR}}}\right)^{\frac{1}{2}}. \tag{37}$$

For the CD3S system with $P_{\mathrm{FI}}$, $P_{\mathrm{dI}}$, and $\beta$ set, there exist $S_{\mathrm{NR}} \in \mathbf{R}$ and $S_{\mathrm{JR}} \in \mathbf{R}$, such that $\alpha^* = \alpha_{\min} = \alpha_{\max}$, where $\alpha^*$ is the local optimal acquisition threshold coefficient at $L = \beta/2$. It is difficult to solve $\alpha^*$ mathematically based on the above description. In order to solve $\alpha^*$ approximately, the problem is transformed into maximizing the margin of acquisition threshold coefficient under the condition of $S_{\mathrm{NR}} = +\infty$ and $S_{\mathrm{JR}} = +\infty$. The margin of the acquisition threshold coefficient is given by

$$M(\alpha) = \min\{|\alpha - \alpha_{\min}|, |\alpha - \alpha_{\max}|\}. \tag{38}$$

The local optimal acquisition threshold coefficient $\alpha^*$ can be expressed as

$$\alpha^* = \underset{\alpha_{\min} \le \alpha \le \alpha_{\max}}{\arg\max} M(\alpha). \tag{39}$$

According to (36), (37), (38) and (39), $\alpha^*$ is derived as

$$\alpha^* \approx \frac{1}{4} + \frac{\sqrt{2}\mathrm{erfc}^{-1}(P_{\mathrm{FI}}) + \mathrm{erfc}^{-1}(2P_{\mathrm{dI}})}{2\sqrt{\beta}}. \tag{40}$$

### E. BER PERFORMANCE OF DEMODULATION

When $b_k = 1$, the received soft bit values is recorded as $\omega_+$ and its distribution is $\omega_+ \sim N\left(\mu_{\omega_+}, \sigma^2_{\omega_+}\right)$. When $b_k = -1$, the received soft bit values is recorded as $\omega_-$ and its distribution is $\omega_- \sim N\left(\mu_{\omega_-}, \sigma^2_{\omega_-}\right)$. During demodulation, $\beta$ chips in each bit of the received signal are aligned with the local chaotic spreading sequence, i.e., $L = \beta$. According to (18) and (19), it can be obtained that

$$\mu_{\omega_+} = E_{\mathrm{b}}, \tag{41}$$

$$\mu_{\omega_-} = -E_{\mathrm{b}}, \tag{42}$$

$$\sigma^2_{\omega_+} = \sigma^2_{\omega_-} = \frac{E_{\mathrm{b}}^2}{2}\left(\frac{1}{S_{\mathrm{NR}}} + \frac{1}{\beta S_{\mathrm{JR}}}\right). \tag{43}$$

The probability density function of $\omega_+$ and $\omega_-$ can be expressed as

$$f_+(\omega_+) = \frac{1}{\sqrt{2\pi}\delta_{\omega_+}}\exp\left(-\frac{(\omega_+ - E_{\mathrm{b}})^2}{2\delta^2_{\omega_+}}\right), \tag{44}$$

$$f_-(\omega_-) = \frac{1}{\sqrt{2\pi}\delta_{\omega_+}}\exp\left(-\frac{(\omega_- + E_{\mathrm{b}})^2}{2\delta^2_{\omega_+}}\right), \tag{45}$$

It is assumed that $b_k$ takes 1 or -1 with equal probability (i.e., $P(1) = P(-1) = 0.5$), and the decision threshold is set to 0. Then, the BER of demodulation is derived as

$$\begin{aligned} P_e &= P\left(-1/1\right)P(1) + P\left(1/-1\right)P(-1) \\ &= \frac{1}{2}\int_{-\infty}^{0} f_+(\omega_+)\mathrm{d}\omega_+ + \frac{1}{2}\int_{0}^{\infty} f_-(\omega_-)\mathrm{d}\omega_- \\ &= \int_{-\infty}^{0} \frac{1}{\sqrt{2\pi}\delta_{\omega_+}}\exp\left(-\frac{(\omega_+ - E_{\mathrm{b}})^2}{2\delta^2_{\omega_+}}\right)\mathrm{d}\omega_+ \\ &= \frac{1}{2}\mathrm{erfc}\left(\frac{E_{\mathrm{b}}}{\sqrt{2}\delta_{\omega_+}}\right) \\ &= \frac{1}{2}\mathrm{erfc}\left[\left(\frac{1}{S_{\mathrm{NR}}} + \frac{1}{\beta S_{\mathrm{JR}}}\right)^{-\frac{1}{2}}\right]. \end{aligned} \tag{46}$$

Equation (46) shows that BDCS-based CD3S system has the same anti-jamming capacity as DSSS system.

## V. NUMERICAL RESULTS

The performance evaluation focuses on the following aspects:

1) Simulate synchronization performance under different SNR and SIR conditions. Compare the numerical simulation results with the theoretical values of false alarm probability, detection probability, and local optimal acquisition threshold coefficient;
2) Compare the anti-interception performance of the transmitted CD3S signals in the PAS system, fixed CD3S system, semi-blind demodulation system, and BDCS-based system;
3) Compare the BER performance between PAS system, fixed CD3S system, semi-blind demodulation system, and BDCS-based system.

In all simulations, the spreading factor $\beta$ is set to 1000. The system initial value $c_{0,1}$ is set to 0.48. The first chaotic map is Tent map which is given in (3). The Tent map parameter $q$ is set to 0.65. The second chaotic map is Logistic map which is given in (4). The probability density function of the Logistic chaotic sequence is given by [32]

$$\rho(c) = \left(\pi\sqrt{1 - c^2}\right)^{-1}, \quad c \in (-1, 1). \tag{47}$$

Substituting (47) into (14), it can be obtained that $P_{\mathrm{c}} = 0.5$.

### A. NUMERICAL ANALYSIS OF SYNCHRONIZATION PERFORMANCE

Fig. 4 shows the output of the correlator when the received signal is acquired. In Fig. 4(a), the received signal that originally lags behind the local chaotic sequence is acquired by the backward FDMF. In Fig. 4(b), the received signal that originally leads the local chaotic sequence is acquired by the forward FDMF. Fig. 4 indicates that the synchronization approach based on BDCS can acquire the aperiodic CD3S signal regardless of whether the received signal is leading or lagging behind the local chaotic sequence.

Fig. 5 shows the receiver operating characteristic (ROC) curves based on theory and simulation for white Gaussian noise and narrowband jamming with different powers. The simulation is run for $10^4$ times. The unit of SNR and SJR is dB in Fig. 5. The theoretical analysis of false alarm probability and detection probability is verified by numerical simulation results in Fig. 5.

Fig. 6 shows the curves of detection probability and false alarm probability based on the acquisition threshold coefficient for white Gaussian noise and narrowband jamming with different powers. In Fig.6, $P_{\mathrm{d}}$ represents the detection probability when the number of aligned chips is $L = \beta/2$. The unit of SNR and SJR is dB in Fig. 6. As the acquisition threshold coefficient $\alpha$ increases, the false alarm probability

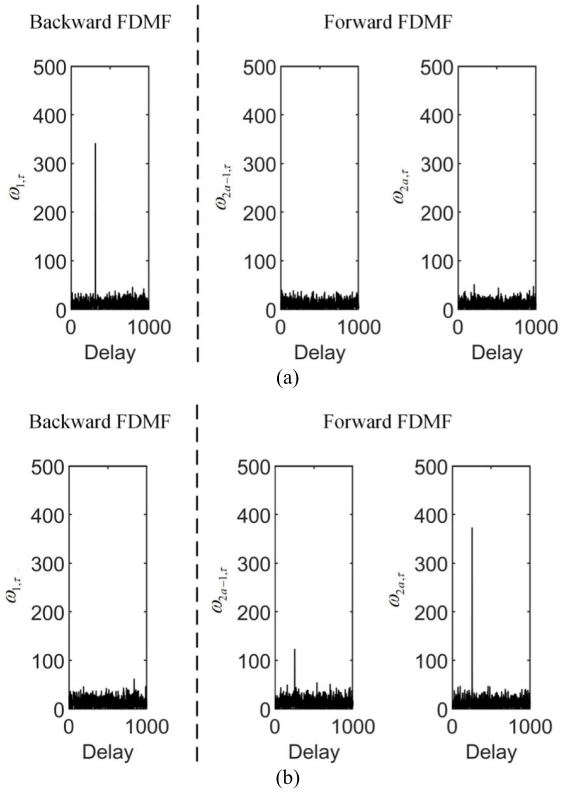


**FIGURE 4.** The output of the correlator when the received signal is acquired. (a) The received signal lags behind the local chaotic sequence ($\tau > 0$). (b) The received signal leads the local chaotic sequence ($\tau < 0$).

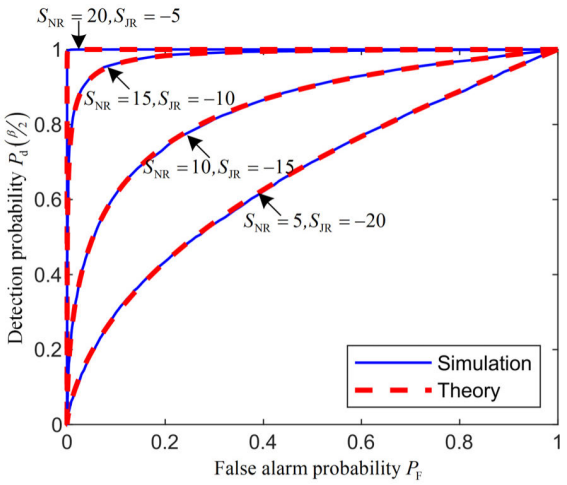


**FIGURE 5.** ROC curves for white Gaussian noise and narrowband jamming with different powers.

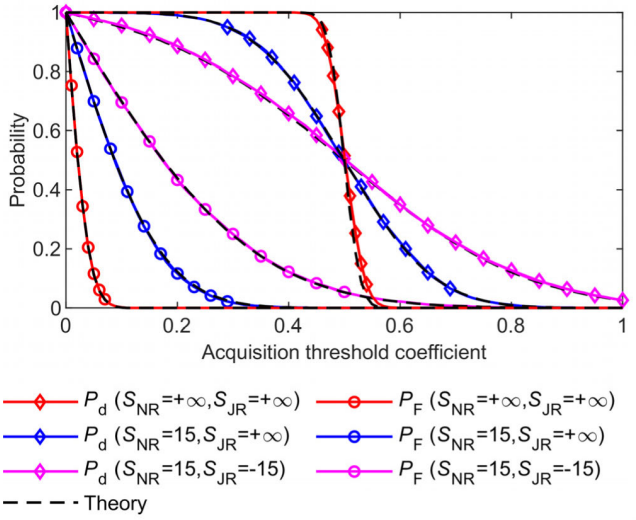


**FIGURE 6.** Curves of detection probability and false alarm probability based on the acquisition threshold coefficient.

and detection probability show a global downward trend. For $\alpha \in [0, 0.5]$, as the power of white Gaussian noise and jamming increases, the curves of false alarm probability and detection probability gradually approach.

In order to further analyze the influence of the acquisition threshold coefficient $\alpha$ on the synchronization performance, Fig. 7 shows the superior limit and inferior limit curves of the acquisition threshold coefficient based on the SNR. In Fig. 7, only white Gaussian noise is considered (i.e., $S_{JR} = +\infty$), the false alarm probability index is set as $P_{FI} = 0.001$ and the detection probability index is set as $P_{dI} = 0.999$. In Fig. 7, the detection probability is analyzed and simulated under the condition of $L = \beta/2$. The curves of detection probability and false alarm probability based on $\alpha$ are obtained under a series of $S_{NR}$ values. Then, the maximum value of $\alpha$ which satisfies $P_{dI}$ is taken as the simulation value of $\alpha_{max}$, and the minimum value of $\alpha$ which satisfies $P_{FI}$is taken as the simulation value of $\alpha_{min}$.

In Fig. 7, the numerical simulation verifies the theoretical analysis of $\alpha_{max}$ and $\alpha_{min}$ under the condition of no jamming. The false alarm probability index $P_{FI}$ is satisfied in the area above the $\alpha_{min}$ curve, and the detection probability index $P_{dI}$ is satisfied in the area below the $\alpha_{max}$ curve. The curves of $\alpha_{max}$ and $\alpha_{min}$ intersect at $S_{NR} = 19.7$dB. For $S_{NR} \geq 19.7$dB, there is $\alpha_{max} \geq \alpha_{min}$, and $\alpha \in [\alpha_{min}, \alpha_{max}]$can satisfy the $P_{FI}$ and the $P_{dI}$. For $S_{NR} < 19.7$dB, there is $\alpha_{max} \leq \alpha_{min}$, and no $\alpha$ can satisfy $P_{FI}$ and $P_{DI}$. Thus, when $\alpha_{max}$ and $\alpha_{min}$ intersect, their value is the actual value of local optimal acquisition threshold coefficient $\alpha^*$. Under the actual value of $\alpha^*$, the noise margin of the receiver is the largest and equal to 19.7dB. The theoretical approximation of $\alpha^*$ obtained from (40) is also shown in Fig. 7. The theoretical approximation of $\alpha^*$ intersects $\alpha_{max}$ at $S_{NR} = 19.9$dB, i.e., the noise margin of the receiver is 19.9dB under the theoretical approximation of $\alpha^*$.The theoretical approximation of $\alpha^*$ only reduces the noise margin of the receiver by 0.2dB. Therefore, (40) is an effective approach to approximately calculate $\alpha^*$ under the condition of no jamming.

Fig. 8 shows the superior limit and inferior limit curves of the acquisition threshold coefficient based on the SJR, where SNR is set to 22dB and 25dB, $P_{FI} = 0.001$, $P_{dI} = 0.999$. In Fig. 8, the detection probability is analyzed and simulated

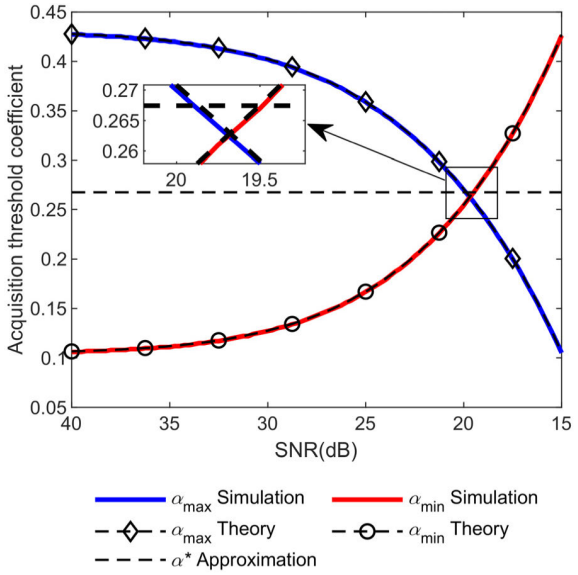


**FIGURE 7.** Superior limit and inferior limit curves of the acquisition threshold coefficient based on the SNR (Index: $P_{FI} = 0.001$, $P_{DI} = 0.999$).

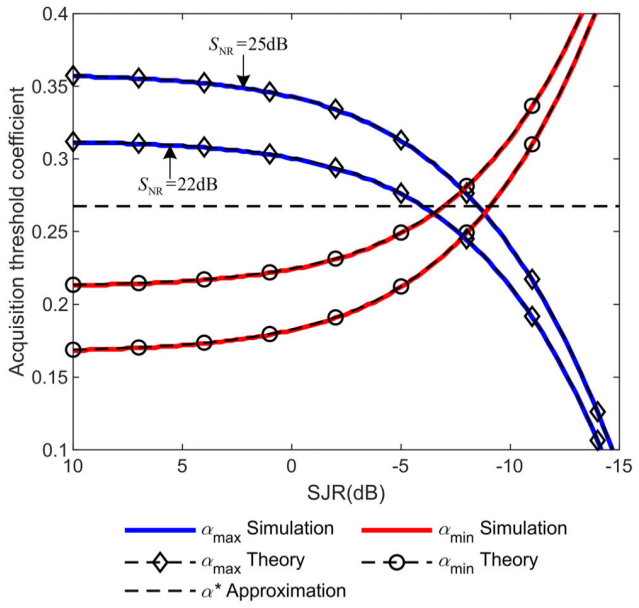


**FIGURE 8.** Superior limit and inferior limit curves of the acquisition threshold coefficient based on the SJR (Index: $P_{FI} = 0.001$, $P_{DI} = 0.999$).

under the condition of $L = \beta/2$. The method to obtain the simulation value is similar to that in Fig. 7. The theoretical analysis of $\alpha_{\max}$ and $\alpha_{\min}$ is verified in the presence of white Gaussian noise and jamming. Table 2 shows the jamming margin of the receiver under the actual value and theoretical approximation of $\alpha^*$ in Fig. 8. For $S_{NR} = 25$dB, the theoretical approximation of $\alpha^*$ reduces the jamming margin of the receiver by 0.25dB. For $S_{NR} = 22$dB, the theoretical approximation of $\alpha^*$ reduces the jamming margin of the receiver by 0.5dB. Therefore, (40) is an effective approach to approximately calculate $\alpha^*$ in the presence of white Gaussian noise and jamming. In addition, Fig. 8 illustrates that the proposed synchronization approach has strong anti-jamming capacity.

**TABLE 2.** Jamming margin under the actual value and theoretical approximation of $\alpha^*$.

| | Jamming margin (dB) | |
|---|---|---|
| | Actual value ($\alpha^*$=0.263) | Approximation ($\alpha^*$=0.267) |
| $S_{NR}$=25dB | -8.75 | -8.5 |
| $S_{NR}$=22dB | -6.5 | -6 |

Fig. 9 shows the curves of detection probability and false alarm probability based on SNR. Fig. 10 shows the curves of detection probability and false alarm probability based on SJR. In these two figures, the detection probability is the global detection probability $P_D$ expressed by (34), and the acquisition threshold coefficient $\alpha$ is set to the approximate value of $\alpha^*$ in Table 2, i.e., $\alpha = 0.267$. In Fig. 9, SJR is set to $+\infty$. In Fig. 10, the SNR is set to 20dB. In Fig. 9, as the SNR decreases, the global detection probability $P_D$ first gradually decreases and then gradually increases, and the false alarm probability $P_F$ gradually increases to equal the global detection probability. The reason for the phenomenon shown in Fig 9 is that as the power spectral density of the white Gaussian noise increases, the probability that the cross-correlation value of the white Gaussian noise and the chaotic sequence exceeds the autocorrelation value of the chaotic sequence increases. Fig. 10 shows a similar phenomenon to Fig. 9 for similar reasons. Fig.10 shows that the proposed synchronization approach has strong anti-jamming ability. Nevertheless, it should be noted that proposed synchronization approach shows strong dependence on the values of SNR, providing proper synchronization properties in terms of $P_D$ and $P_F$ only when SNR $>$ 20dB.

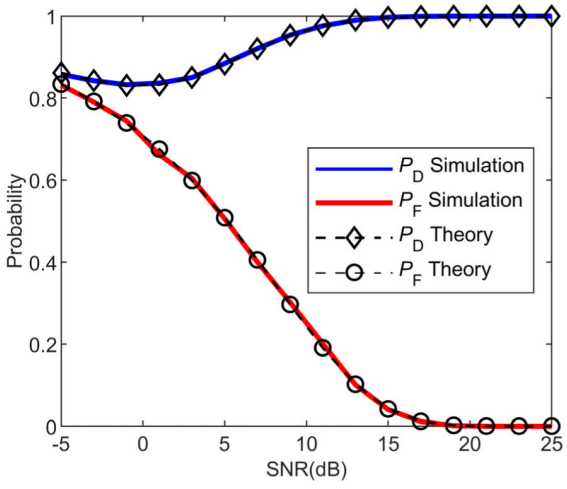


**FIGURE 9.** Curves of global detection probability and false alarm probability based on SNR ($\alpha = 0.267$, $S_{JR} = +\infty$).

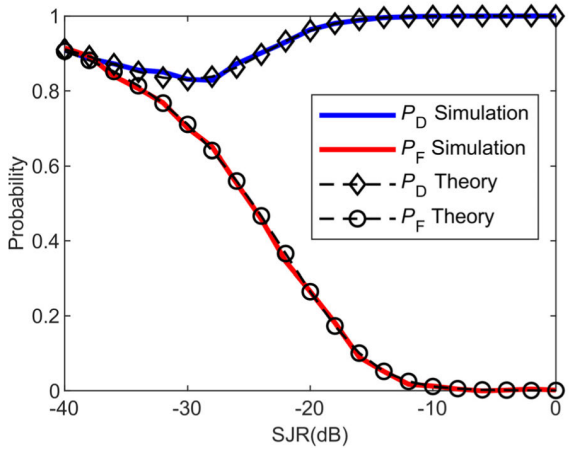


**FIGURE 10.** Curves of global detection probability and false alarm probability based on SJR ($\alpha = 0.267$, $S_{NR} = 20$dB).

### B. COMPARISON OF ANTI-INTERCEPTION PERFORMANCE

Taking advantage of the periodicity of PN codes, noncooperative receivers intercept the spread spectrum signals by the cyclic spectrum density algorithm, the delay-and-multiply algorithm, or the second-order moment of autocorrelation algorithm [7], [33], [34]. In this section, the second moment of the autocorrelation function [34] is selected to compare the anti-interception performance of the transmitted CD3S signal among PAS system, fixed CD3S system, semi-blind demodulation system, and BDCS-based system.

The transmitted signals in the four CD3S systems are generated as follows:

1) In the PAS system, the CD3S signal is transmitted together with an additive pilot with the same power 13] and the pilot is a truncated Logistic chaotic sequence with a period of $\beta$ chips;
2) In the fixed CD3S system, each message bit is spread by a fixed chaotic sequence which is the Logistic chaotic sequence with a period of $\beta$ chips [17];
3) In the semi-blind demodulation system, each message bit is spread by a unique Logistic chaotic sequence 24];
4) In the BDCS-based system, the generation of the CD3S signal is shown in Section II.

In the second-order moment analysis of autocorrelation, the noisy CD3S signal with a length of $101 \times \beta$ chips is analyzed, and the CD3S signal is divided into 100 segments with a length of $2\beta$ chips and 50% overlap. The autocorrelation of the $k$th segment is expressed as

$$R_\tau^k = \frac{1}{2\beta} \sum_{n=0}^{2\beta-1} r(n)\, r(n-\tau) \tag{48}$$

The second-order moment of autocorrelation is estimated by 100 segments as

$$\Phi(\tau) = \mathrm{E}\left[\left(R_\tau^k\right)^2\right] = \frac{1}{100} \sum_{k=1}^{100} \left(R_\tau^k\right)^2 \tag{49}$$

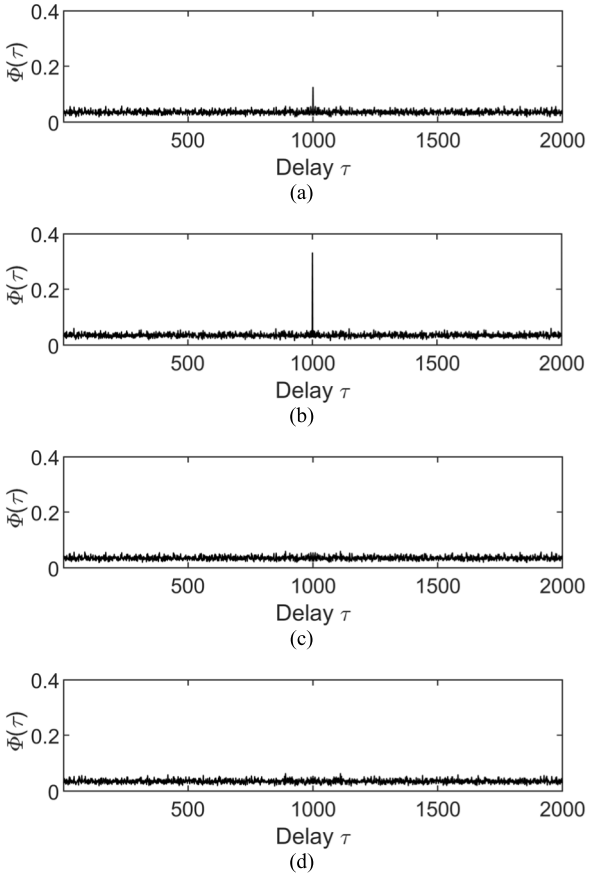


**FIGURE 11.** The second-order moment of autocorrelation of the four CD3S signals ($S_{NR} = 15$dB, $S_{JR} = +\infty$). (a) Transmitted signal in PAS system. (b) Transmitted signal in Fixed CD3S system. (c) Transmitted signal in semi-blind demodulation system. (d) Transmitted signal in BDCS-based system.

Fig. 11 compares the second-order moment of autocorrelation of the four transmitted signals. In Fig. 11, SNR is set to 15dB and SJR is set to $+\infty$. Due to the periodicity of pilot signal and fixed chaotic sequence, obvious peaks appear in Fig. 11(a) and Fig. 11(b). In the PAS system, the pilot power is half of the transmission power, so the peak value in Fig. 11(a) is lower than that in Fig. 11(b). The transmitted signals in the semi-blind demodulation system and the BDCS-based system are aperiodic. Therefore, there is no obvious peak in Fig. 11(c) and Fig. 11(d).

To compare the anti-interception performance of the four transmitted signals more rigorously, Fig. 12 shows peak to average ratio (PAR) curves of $\Phi(\tau)$ based on SNR. To ensure resolution at low PAR values, the ordinate axis of Fig. 12 uses a logarithmic scale. In the PAS system and fixed CD3S system, the PAR of $\Phi(\tau)$ increases with the increase of SNR, which makes the transmitted signals easily intercepted. In the semi-blind demodulation system and BDCS-based system, the PAR of $\Phi(\tau)$ maintains a low value, which indicates that the transmitted signals in these two systems have stronger anti-interception capabilities.

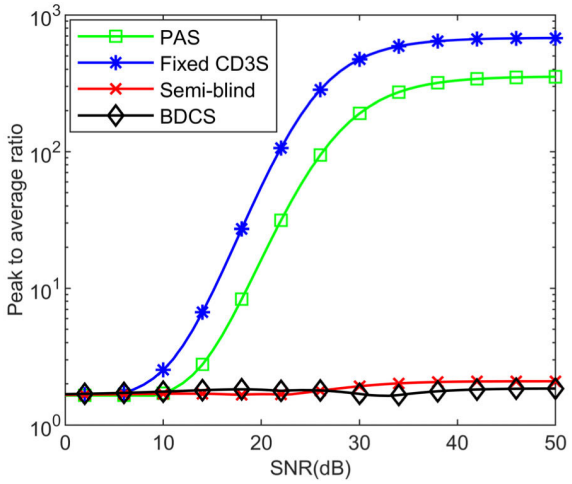


**FIGURE 12.** PAR curves of $\Phi(\tau)$ based on SNR for the four kinds of transmitted signals.

### C. COMPARISON OF BER PERFORMANCE

To compare the BER performance among PAS system, fixed CD3S system, semi-blind demodulation system, and BDCS-based system, Fig. 13 shows the BER curves of the four systems based on SNR. The generation of the four transmitted signals is shown in section V-B. In the PAS system, fixed CD3S system, and BDCS-based system, the received signal is demodulated by the corresponding locally synchronized chaotic sequence. Considering the Gaussian distribution of noise, the received signal is demodulated by UKF [24] in the semi-blind demodulation system, and we assume that the prior knowledge of noise power has been obtained.

In Fig. 13, the BER of the semi-blind demodulation system is much higher than that of the other three systems. The reason is that the receiver of the semi-blind demodulation system estimates the chaotic sequence from the received signal instead of directly generating the same local chaotic sequence as the transmitter. Reference [26] analyzed the mean square error (MSE) of chaotic sequence estimation. The MSE is equal to -20dB when $P_c/N_0 = 0$dB (i.e., $S_{NR} = 30$dB for $\beta = 1000$), and the MSE increases by 4dB whenever the $P_c/N_0$ decreases by 3dB [26]. In semi-blind demodulation system, the error of the chaotic sequence estimation results in the poor BER performance at low SNR. The advantage of semi-blind demodulation is that it does not require full knowledge of the chaotic system in transmitter. Due to this advantage, non-cooperative receiver can break the CD3S system by semi blind demodulation approach. The PAS approach, fixed CD3S approach, and BDCS-based approach generate the same chaotic sequence as the transmitter locally and require all knowledge of the chaotic system in transmitter, which are more suitable for cooperative receivers. If the knowledge of the chaotic system is not complete and accurate, these three approaches will not be able to demodulate the information due to the sensitivity of the chaotic system to initial values and parameters. The BER performance of PAS system is 3 dB lower than that of fixed CD3S system and BDCS-based system. The reason is that only half of the power is used to transmit message bits in the PAS system. The fixed CD3S system and the BDCS-based system have the best BER performance, their simulation values are consistent with the theoretical values in (46).

To analyze the influence of jamming on the BER, Fig. 14 shows the BER curves of the four systems based on the SJR. In order to analyze the influence of jamming separately, the SNR of each system is set to the value when their BER is equal to $10^{-4}$ in Fig. 13. Therefore, in Fig. 14, the SNR of the fixed CD3S system and BDCS-based system is set to 8.4dB, the SNR of the PAS system is set to 11.4dB, the SNR of the semi-blind demodulation system is set to 26dB. In Fig. 14, the BER of the semi-blind demodulation system is much higher than that of the other three systems. The BER of PAS system, fixed CD3S system and

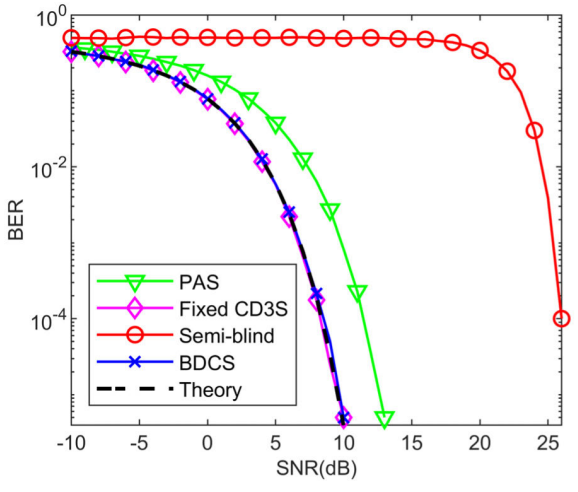


**FIGURE 13.** BER curves based on SNR.

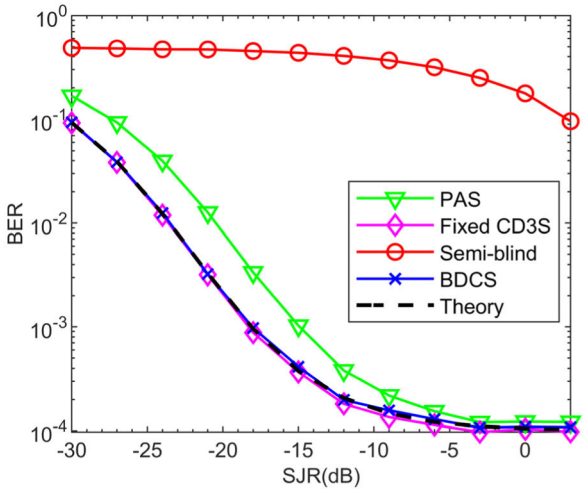


**FIGURE 14.** BER curves based on the SJR.

BDCS-based system decreases to $10^{-4}$ with the increase of SJR. The BER performance of the PAS system is 3 dB lower than that of fixed CD3S system and BDCS-based system. The above phenomenon occurs for reasons similar to those in Fig. 13.

Fig. 13 shows that the BER of BDCS-based system is $5 \times 10^{-6}$ when $S_{\mathrm{NR}} = 10$dB, and the BER is $10^{-4}$ when $S_{\mathrm{NR}} = 8.4$dB. According to Fig. 9, when $S_{\mathrm{NR}} = 10$dB, $P_{\mathrm{D}}$ equals to 0.966, and $P_{\mathrm{F}}$ equals to 0.242. When $S_{\mathrm{NR}} = 8.4$dB, $P_{\mathrm{D}}$ equals to 0.944, and $P_{\mathrm{F}}$ equals to 0.329. Under low SNR conditions, the BDCS-based system has a BER performance not worse than the one corresponding with fixed CD3S system, but the false alarm probability and detection probability performance are relatively poor. The reason is that the local chaotic sequence has been aligned with the received signal in the demodulation stage, and the bit error will only occur when the sign of the correlator output changes. However, in the acquisition phase, when the local chaotic sequence is aligned with the received signal, there will be missed detection if the output of the correlator is less than the acquisition threshold. When the SNR is low, synchronization will take longer due to missed detections and false alarms. Using more correlators to perform parallel searches from different initial values can reduce the synchronization time, but the receiver structure will also be more complicated. Thus, it should be emphasized again that the proposed synchronization approach shows strong dependence on the values of SNR, providing a proper synchronization properties in terms of $P_{\mathrm{D}}$ and $P_{\mathrm{F}}$ only when SNR $>$ 20dB.

## VI. CONCLUSION

In order to construct a CD3S system with low intercept probability and anti-jamming capacity, the paper proposed a synchronization approach based on BDCS. In the approach, the transmitted signal is aperiodic, which ensures the anti-interception performance. The false alarm probability, the detection probability and the BER are analyzed theoretically. The local optimal acquisition threshold coefficient for synchronization is obtained approximately. Numerical simulations verified these theoretical analyses. Given the simulation conditions in this paper, the approximate solution to the local optimal acquisition threshold coefficient reduces the anti-noise and anti-jamming capacity of synchronization within 0.5dB, which indicates that the approximate solution is effective. The anti-interception performance and BER performance of the PAS system, fixed CD3S system, semi-blind demodulation system, and the proposed BDCS-based system were compared in this paper. Numerical simulation showed that the anti-interception performance and BER performance of the BDCS-based system are the best among the four systems under the conditions of proper synchronization achieved.

The proposed synchronization approach may only have $\beta/2$ chips aligned during correlation search, which limits the anti-noise and anti-jamming capacity of synchronization. The future research will improve the synchronization approach so that more chips can be aligned during correlation search. In addition, more complex channel environment will be considered in future research.

## REFERENCES


[1] A. Mesloub, A. Boukhelifa, O. Merad, S. Saddoudi, A. Younsi, and M. Djeddou, "Chip averaging chaotic ON–OFF keying: A new non-coherent modulation for ultra wide band direct chaotic communication," *IEEE Commun. Lett.*, vol. 21, no. 10, pp. 2166–2169, Oct. 2017.

[2] Y. Fu, S. Guo, and Z. Yu, "The modulation technology of chaotic multi-tone and its application in covert communication system," *IEEE Access*, vol. 7, pp. 122289–122301, 2019.

[3] T. J. Wren and T. C. Yang, "Orthogonal chaotic vector shift keying in digital communications," *IET Commun.*, vol. 4, no. 6, pp. 739–753, Apr. 2010.

[4] F. Liu, L. Wang, J. Xie, Y. Wang, and Z. Zhang, "MP-WFRFT and chaotic scrambling aided directional modulation technique for physical layer security enhancement," *IEEE Access*, vol. 7, pp. 74459–74470, 2019.

[5] G. Heidari-Bateni and C. D. McGillem, "A chaotic direct-sequence spread-spectrum communication system," *IEEE Trans. Commun.*, vol. 42, no. 234, pp. 1524–1527, Feb. 1994.

[6] U. Parlitz and S. Ergezinger, "Robust communication based on chaotic spreading sequences," *Phys. Lett. A*, vol. 188, no. 2, pp. 146–150, May 1994.

[7] J. Yu and Y.-D. Yao, "Detection performance of chaotic spreading LPI waveforms," *IEEE Trans. Wireless Commun.*, vol. 4, no. 2, pp. 390–396, Mar. 2005.

[8] Y. Hwang and H. C. Papadopoulos, "Physical-layer secrecy in AWGN via a class of chaotic DS/SS systems: Analysis and design," *IEEE Trans. Signal Process.*, vol. 52, no. 9, pp. 2637–2649, Sep. 2004.

[9] K. Busawon, P. Canyelles-Pericas, R. Binns, I. Elliot, and Z. Ghassemlooy, "A brief survey and some discussions on chaos-based communication schemes," in *Proc. 11th Int. Symp. Commun. Syst., Netw. Digit. Signal Process. (CSNDSP)*, Budapest, Hungary, Jul. 2018, pp. 1–5.

[10] B. Jovic, C. P. Unsworth, G. S. Sandhu, and S. M. Berber, "A robust sequence synchronization unit for multi-user DS-CDMA chaos-based communication systems," *Signal Process.*, vol. 87, no. 7, pp. 1692–1708, Jul. 2007.

[11] G. Kaddoum, D. Roviras, P. Chargé, and D. Fournier-Prunaret, "Robust synchronization for asynchronous multi-user chaos-based DS-CDMA," *Signal Process.*, vol. 89, no. 5, pp. 807–818, May 2009.

[12] A. Tayebi, S. Berber, and A. Swain, "Performance analysis of chaotic DSSS-CDMA synchronization under jamming attack," *Circuits, Syst., Signal Process.*, vol. 35, no. 12, pp. 4350–4371, Dec. 2016.

[13] A. Tayebi, S. Berber, and A. Swain, "A new approach for error rate analysis of wide-band DSSS-CDMA system with imperfect synchronization under jamming attacks," *Wireless Pers. Commun.*, vol. 98, no. 4, pp. 3583–3610, Feb. 2018.

[14] X. Shu, J. Wang, H. Wang, and X. Yang, "Chaotic direct sequence spread spectrum for secure underwater acoustic communication," *Appl. Acoust.*, vol. 104, pp. 57–66, Mar. 2016.

[15] H.-P. Ren, C. Bai, Q. Kong, M. S. Baptista, and C. Grebogi, "A chaotic spread spectrum system for underwater acoustic communication," *Phys. A, Stat. Mech. Appl.*, vol. 478, no. 15, pp. 77–92, Jul. 2017.

[16] G. Mazzini, G. Setti, and R. Rovatti, "Chaotic complex spreading sequences for asynchronous DS-CDMA. I. system modeling and results," *IEEE Trans. Circuits Syst. I, Fundam. Theory Appl.*, vol. 44, no. 10, pp. 937–947, Oct. 1997.

[17] A. Tayebi, S. Berber, and A. Swain, "Security enhancement of fix chaotic-DSSS in WSNs," *IEEE Commun. Lett.*, vol. 22, no. 4, pp. 816–819, Apr. 2018.

[18] Y. Chen, F. He, J. Yan, X. Chen, and Y. Gu, "A smart tracking-based jamming scheme for signals with periodic synchronization sequences," in *Proc. Int. Conf. Wireless Commun. Signal Process. (WCSP)*, Nanjing, China, Nov. 2011, pp. 1–5.

[19] O. Hugues-Salas and K. A. Shore, "An extended Kalman filtering approach to nonlinear time-delay systems: Application to chaotic secure communications," *IEEE Trans. Circuits Syst. I, Reg. Papers*, vol. 57, no. 9, pp. 2520–2530, Sep. 2010.

[20] X. Xu and J. Guo, "A novel unified equalization and demodulation of chaotic direct sequence spread spectrum signal based on state estimation," *Acta Phys. Sinica*, vol. 60, no. 2, 2011, Art. no. 020510.

[21] J. Lin and W. Lin, "Extended Kalman filter-based codec for chaotic communication systems," *Int. J. Bifurcation Chaos*, vol. 24, no. 7, 2014, Art. no. 11450094.
[22] G. Yuan, Y. Wang, P. Chen, and X. Gao, "Demodulation of CD3S signals based on DEKF joint estimation," *Syst. Eng. Electron.*, vol. 40, no. 9, pp. 2119–2123, Sep. 2018.
[23] G. Lu and X. Bo, "Breaking a chaotic direct sequence spread spectrum communication system using interacting multiple model-unscented Kalman filter," *Chaos, Interdiscipl. J. Nonlinear Sci.*, vol. 22, no. 4, Dec. 2012, Art. no. 043122.
[24] X. Xu and J. Guo, "Combined equalization and demodulation of chaotic direct sequence spread spectrum signals for multipath channels," *Circuits, Syst., Signal Process.*, vol. 32, no. 6, pp. 2957–2969, Dec. 2013.
[25] P. Chen, G. Yuan, Y. Wang, and X. Gao, "Demodulation of CD3S signals through mixed Kalman filtering for multipath channel," *J. Huazhong Univ. Sci. Technol. (Natural Sci. Ed.)*, vol. 46, no. 11, pp. 76–80, Nov. 2018.
[26] S. Mukhopadhyay and H. Leung, "Blind system identification using symbolic dynamics," *IEEE Access*, vol. 6, pp. 24888–24903, 2018.
[27] M. Yahia, D. Radi, L. Gardini, and V. Freschi, "Use of chebyshev polynomial Kalman filter for pseudo-blind demodulation of CD3S signals," *Int. J. Control, Autom. Syst.*, vol. 13, no. 5, pp. 1193–1200, Oct. 2015.
[28] T. Li, D. Zhao, Z. Huang, C. Liu, S. Su, and Y. Zhang, "Blind demodulation of chaotic direct sequence spread spectrum signals based on particle filters," *Entropy*, vol. 15, no. 12, pp. 3877–3891, Sep. 2013.
[29] T. Li, D. Zhao, Z. Huang, S. Su, C. Liu, and Z. Zuo, "Breaking chaotic direct sequence spreading spectrum signals under the multipath fading channel," *Circuits, Syst., Signal Process.*, vol. 33, no. 3, pp. 973–986, Mar. 2014.
[30] I. Shaahin Varnosfaderani, M. F. Sabahi, and M. Ataei, "Joint blind equalization and detection in chaotic communication systems using simulation-based methods," *AEU, Int. J. Electron. Commun.*, vol. 69, no. 10, pp. 1445–1452, Oct. 2015.
[31] Y. Zhou, Z. Hua, C.-M. Pun, and C. L. P. Chen, "Cascade chaotic system with applications," *IEEE Trans. Cybern.*, vol. 45, no. 9, pp. 2001–2012, Sep. 2015.
[32] S. Berber and S. Feng, "Theoretical modeling and simulation of a chaos-based physical layer for WSNs," *Int. J. Commun.*, vol. 7, no. 2, pp. 27–34, 2013.
[33] M. Guan and L. Wang, "A novel recognition method for low SNR DSSS signals based on four-order cumulant and eigenvalue analysis," *Chin. J. Electron.*, vol. 24, no. 3, pp. 650–653, Jul. 2015.
[34] B. Shen and J.-X. Wang, "Chip rate and pseudo-noise sequence estimation for direct sequence spread spectrum signals," *IET Signal Process.*, vol. 11, no. 6, pp. 727–733, Aug. 2017.

**GUOGANG YUAN** was born in Sichuan, China, in 1994. He received the B.S. degree in unmanned aerial vehicle engineering from the Mechanical Engineering College, Shijiazhuang, China, in 2016, and the M.S. degree in control science and engineering from the Shijiazhuang Campus of AEU, Shijiazhuang, in 2018, where he is currently pursuing the Ph.D. degree in control science and engineering. His research interests include the areas of chaotic communication and physical layer security.

**ZILI CHEN** was born in Shanxi, China, in 1964. He received the B.S. degree from the Mechanical Engineering College, Shijiazhuang, China, in 1984, and the M.S. degree from the Nanjing University of Science and Technology, Nanjing, China, in 1987. He is currently a Full Professor with the Shijiazhuang Campus of AEU, Shijiazhuang. His research interests include the areas of UAV-assisted communication and signal processing.

**XIJUN GAO** received the B.S. degree in electronic information engineering from Dalian Maritime University, China, in 2009, and the M.S. degree in communication and information system and the Ph.D. degree in control science and engineering from the Mechanical Engineering College, Shijiazhuang, China, in 2011 and 2015, respectively. He is currently pursuing the degree in UAV communication technology.

**JIANGYAN HE** received the B.S. and M.S. degrees in mathematics from Hebei Normal University, Shijiazhuang, China, in 2005 and 2008, respectively. She is currently a Lecturer with the Shijiazhuang Campus of AEU, Shijiazhuang. Her research interests include the areas of the basic theory of nonlinear functional analysis and anti-jamming communication.

**HONGXIA JIA** received the B.S. degree in electronic information engineering and the M.S. degree in information and communication system from Dalian Maritime University, China, in 2009 and 2011, respectively. She is currently pursuing the degree in communication application.